# CFD modeling of slurry bubble column reactor for Fischer-Tropsch synthesis

Andrey A. Troshko
ANSYS Inc., Fluid Business Unit, USA

## ABSTRACT

Industrial bubble column reactor for Fischer-Tropsch (FT) synthesis includes complex hydrodynamic, chemical and thermal interaction of three material phases: population of bubbles of different sizes, liquid and catalyst particles suspended in liquid. To simulate FT bubble column, a Computational Fluid Dynamics model is described here. The model is based on Eulerian multifluid formulation and accounts for the following important phenomena. Turbulence is modeled by $k - \varepsilon$ model. Bubble size distribution is predicted by the Population Balance (PB) method. Experimentally observed influence of catalyst particle concentration on bubble size distribution is theorized to be linked to catalyst particle induced modification of turbulent dissipation rate. A simple scaling modification to dissipation rate is proposed to model this influence. Additional mass conservation equations are introduced for chemical species associated with phases. Heterogeneous and homogeneous reaction rates representing simplified FT synthesis are taken from literature and incorporated in the model.

The model has been tested against experimental results on lab scale bubble columns. Good agreement was observed for bubble size distribution and gas holdup for bubble columns operating in bubble and churn turbulent regimes. Finally, a full model including chemical species transport was applied to industrial scale bubble column. Predicted hydrocarbon production rate was compared to one dimensional lumped parameter model.

*Keywords:*    Fischer-Tropsch synthesis, heterogeneous reactions, gas holdup, mass transfer, bubble column reactor

**INTRODUCTION**

Recent advances in implementation of Population Balance methods into multidimensional CFD models for bubble columns [1] offer an attractive opportunity to build a mechanistic predictive tool for industrial bubble column reactors. One important application of bubble column reactors is Fischer-Tropsch (FT) synthesis perceived as alternative method of hydrocarbon generation from coal-derived syngas also known as indirect coal liquefaction technology [2]. Conceptual design of FT reactor is depicted in Figure 1. The main features related to CFD modeling are as follows. Syngas, which is a mixture of CO and $H_2$, is introduced through the bottom plate of reactor into liquid slurry. Syngas flow rate is high so churn turbulent regime is typical. This means that bubble population consists of bubbles with different sizes. The slurry consists of liquid and catalyst particles. Gas species diffuse from interface of bubbles into slurry. The rate of this diffusion depends on bubble size. While in slurry chemical species diffuse towards catalyst particle and react at its surface. The simplest FT synthesis reaction in slurry phase is $CO + H_2 \rightarrow CH_2 + H_2O$. This reaction is exothermal so heat exchanger is always present in reactor to remove the heat.

Therefore, to adequately model all important aspects of FT system, the multifluid CFD model must account for the following physical phenomena. First, evolution of bubble size distribution must be predicted since it determines gas holdup and interfacial area density, which is important for gas absorption rate calculation. Second, the correct drag force model is important as it, together with bubble size distribution, determines gas phase distribution. Third, experimentally observed strong influence of catalyst particles in slurry on the gas holdup must be accounted for. Fourth, transport of chemical species within gas and slurry phase must be introduced together with heterogeneous (absorption of chemical species from bubbles to slurry) and homogeneous (FT synthesis reaction) reaction rates. Fifth the, transport of reaction heat and removal of this heat by heat exchanger are important. Sixth, influence of heat exchanger on drag law and bubble size distribution should be accounted for if effective porosity of internal reactor structures is small enough. In our view such model would allow scale up investigations and finding of optimal regimes of operation. Buildup of such a model is an aim of the present study.
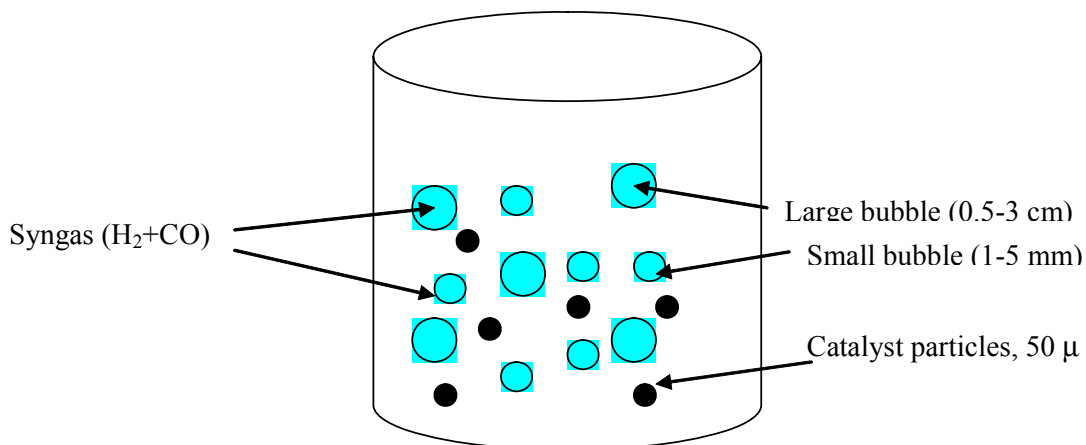


Figure 1: Visual representation of generic FT reactor.

## MODELING APPROACH

The following assumptions were made. First, the slurry is assumed to be perfectly mixed. This is true if Stokes number of catalyst particles is small. Second, heat transfer is neglected and chemical reactions are assumed not to affect material properties of gas and slurry phases. Consequently, the heat transfer is neglected. Third, reaction rate is assumed to be limited by a slurry side diffusion.

The dynamics of syngas-slurry system is described by two-phase Eulerian model. The continuity, momentum and species mass conservation equations for the phase $q$ are:

$$\frac{\partial}{\partial t}\left(\alpha_q \rho_q\right) + \nabla \cdot \left(\alpha_q \rho_q \vec{v}_q\right) = -\dot{m}_{qp} \qquad (1)$$

$$\frac{\partial}{\partial t}\left(\alpha_q \rho_q \vec{v}_q\right) + \nabla \cdot \left(\alpha_q \rho_q \vec{v}_q \vec{v}_q\right) = -\alpha_q \nabla p + \nabla \cdot \overline{\overline{\tau}}_q + \alpha_q \rho_q \vec{g}_q + K_{pq}\left(\vec{v}_p - \vec{v}_q\right) + \dot{m}_{pq}\vec{v}_{pq} \quad (2)$$

$$\frac{\partial}{\partial t}\left(\alpha_q \rho_q Y_q^j\right) + \nabla \cdot \left(\alpha_q \rho_q \vec{v}_q Y_q^j\right) = \nabla\left(\alpha_q \rho_q D_q^j \nabla Y_q^j\right) + R_q^j - R_{qp}^{ij} \quad (3)$$

Closures are required for many terms on right hand sides of these equations. These will be described next.

Interfacial mass transfer terms account for heterogeneous chemical reactions happening at bubble-slurry interface. According to FT reactor description [3], the bubble chemical composition is CO+$H_2$. As bubbles are floating through slurry, both species CO and $H_2$ are diffusing from the bubble interface into the slurry (gas absorption process):

$$CO_g \rightarrow CO_s \quad (4a)$$

$$H_{2g} \rightarrow H_{2s} \quad (4a)$$
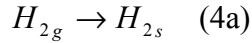
The rate of the absorption reaction is [3]:

$$R_{gs}^{ij} = \begin{cases} \left(k_L a\right)M_w^j\left(\dfrac{c_g^j}{H_g^i} - c_s^j\right), & \text{if } \alpha_g \alpha_s > 0.01, \, j = CO, H_2 \\ 0, & \text{if } \alpha_g \alpha_s \leq 0.01 \end{cases} \qquad (5)$$

The specific values of volumetric mass transfer coefficient and Henry constant for industrial scale FT reactor are given by [3] for the small and large bubbles. Once in slurry phase, hydrogen and carbon monoxide diffuse towards the surface of the catalyst particles and react. The FT synthesis reaction in its simplest form:

$$CO + 2H_2 \rightarrow CH_2 + H_2O \qquad (6)$$

The FT homogeneous reaction rate is expressed as [4]:

$$R_s = ac_s^{CO}c_s^{H_2}\left(1 + b \cdot c_s^{CO} \cdot c_s^{CO}\right)^{-1}\rho_{cat}\alpha_{cat} \, [\text{kmol/m}^3/\text{sec}] \qquad (7)$$

The coefficients $a$ and $b$ are expressed as:

$$a = 8.8533 \cdot 10^{-16} \exp\left(4494.41\left(1/493.15 - 1/T_s\right)\right)\left(T_s R\right)^2 M_w^{CO} M_w^{H_2} \, [\text{m}^6/\text{sec/kg}_{cat}/\text{kmol}] \quad (8a)$$
$$b = 2.226 \cdot 10^{-5} \exp\left(8326\left(1/493.15 - 1/T_s\right)\right)\left(T_s R\right) M_w^{CO} \, [\text{m}^3/\text{kmol}] \quad (8b)$$

The turbulence $k - \varepsilon$ equations are solved for the mixture phase:

$$\frac{\partial}{\partial t}\left(\rho_m k_m\right) + \nabla \cdot \left(\rho_m \vec{v}_m k_m\right) = -\nabla \cdot \left(\frac{\mu_{t,m}}{\text{Pr}_m} \nabla k_m\right) + G_m - \rho_m \varepsilon_m \quad (9)$$

$$\frac{\partial}{\partial t}\left(\rho_m \varepsilon_m\right) + \nabla \cdot \left(\rho_m \vec{v}_m \varepsilon_m\right) = -\nabla \cdot \left(\frac{\mu_{t,m}}{\text{Pr}_\varepsilon} \nabla \varepsilon_m\right) + \frac{\varepsilon_m}{k_m}\left(C_{\varepsilon 1} G_{k,m} - C_{\varepsilon 2} \rho_m \varepsilon_m\right) \quad (10)$$

The drag coefficient is calculated as [5]:

$$K_{gs} = K_{sg} = 0.125 \rho_s A''_{gs} C_{gs}^d \left|\vec{v}_{gs}\right| \quad (11)$$

The churn-turbulent regime is characterized by continuous bubble size distribution. Bubbles coalesce and breakup so size distribution evolves in space and time. Recently, a Population Balance (PB) method was introduced to predict evolution of the bubble size distribution [1]. In PB method the bubble size range is subdivided into several discrete bubble classes. Each class represents a fraction of total bubbles with size within certain size range. The volume fraction of class $i$ is determined as:

$$\alpha_{gi} = \alpha_g f_i \equiv \frac{\pi d_i^3}{6} n_i \quad (12)$$

and bubble class mass conservation equation is:

$$\frac{\partial\left(\alpha_g \rho_g f_i\right)}{\partial t} + \nabla \cdot \left(\alpha_g \rho_g \vec{v}_{gi} f_i\right) = S_{gi} - \dot{m}_{gsi} \quad (13)$$

Taking into account equations 1, 12 and 13, the relation between collective gas velocity and velocities of bubble classes is:

$$\vec{v}_g = \sum_{i=1}^{N_i} \vec{v}_{gi} f_i \quad (14)$$

Equation 14 means that gas velocity $\vec{v}_g$ used in momentum equations 1, 2 and 3 is center of volume velocity of entire bubble size distribution. Source term $S_{gi}$ represents net contribution of break up and coalescence effects. This source is calculated from breakup and coalescence probability kernels [1]. The coalescence kernel was taken from the work

of Luo [6]. The breakup kernel was adopted from Lehr et al. [7] and modified. The physical foundation of the breakup kernel is based on the assumption that breakup event is determined by ratio between turbulent shear and surface tension force assuming near cylindrical bubble shape before breakup. Kinetic energy of eddy hitting the bubble is distributed exponentially which is equivalent to normal eddy velocity distribution valid for inertial turbulence scale [8]. Therefore, bubble size distribution $P(\lambda, d_i, d_j)$ of bubble with diameter $d_i$ hit by eddy of size $\lambda$ and breaking into two bubbles with smaller diameter $d_j$ (larger of diameters is determined from mass conservation), will be exponential distribution of ratio of energy per slurry mass unit $e_{crit}$ required to break the bubble and average kinetic energy of eddy $\bar{e}$ :

$$P(\lambda, d_i, d_j) \propto \left(\frac{e_{crit}}{\bar{e}}\right) \cdot \exp\left(-\left(\frac{e_{crit}}{\bar{e}}\right)\right) \quad (15)$$

The critical energy is calculated based on critical Weber number:

$$e_{crit} = \frac{4 We_{crit} \sigma_{sg}}{\rho_s d_j} \quad (16)$$

Lehr et al. [7] adopted $We_{crit} = 1$. The author found that $We_{crit} = 0.1$ produces better match with experimental data and is closer to value $We_{crit} = 0.4$ recommended by Kolev [9].

The averaged turbulent eddy energy $\bar{e}$ is calculated from (Hinze, 1975)

$$\bar{e} = 2(\varepsilon_m d_i)^{2/3} \quad (17)$$

Another feature of the model is that bubble with diameter less than capillary limit diameter

$$d_{i,\min} = 1.15 \frac{\sigma_{sg}^{3/5}}{\rho_s^{3/5} \varepsilon_m^{2/5}} \quad (18)$$

is unbreakable, that is:

$$P(\lambda, d_i < d_{i,\min}, d_j) = 0 \quad (19)$$

The drag coefficient is automatically chosen by algorithm in equation 20 from three drag coefficients. These coefficients are calculated for spherical, distorted and spherical cap bubble (subscripts 1, 2 and 3 respectively) and account for the bubble concentration effect [10]:

$$C_{gs}^d = C_{gs,1}^d \text{ if } C_{gs,1}^d > C_{gs,2}^d)$$
$$\text{else } C_{gs}^d = MIN\left(C_{gs,2}^d, C_{gs,3}^d\right) \quad (20)$$

Equation 11 is valid for arbitrary bubble size distribution assuming drag coefficient does not depend on the bubble size. In churn turbulent regime this assumption is not valid [10]. More general expression can be derived my method analogous to one employed by Ishii and Zuber [10]. For bubble swarm characterized by bubble size distribution $\{f_i, i = 1, N\}$ freely rising in an infinite liquid medium the total drag force density acting on bubble in size group $i$ is equalized by the gravity force:

$$\alpha_g f_i g\left(\rho_s - \rho_g\right) = \frac{1}{8}\rho_s A_{gs,i}'' C_{gs,i}^d U_{gs,i}^2 \quad (21)$$

So using equations 11, 14 and 21, the relation between drag coefficient for the center of volume rise velocity and class drag coefficients is:

$$A_{gs}'' C_{gs}^d = \alpha_g \left[\sum_{i=1}^{N} f_i \left(\frac{\alpha_g f_i}{A_{gs,i}'' C_{gs,i}^d}\right)^{1/2}\right]^{-2} \quad (22)$$

Assuming spherical bubble shape relation between interfacial area density and bubble diameter

$$A_{gs,i}'' = \frac{6\alpha_g f_i}{d_i} \quad (23)$$

So equation 25 reduces to:

$$C_{gs}^d = d_{32}\left[\sum_{i=1}^{N} f_i \left(\frac{d_i}{C_{gs,i}^d}\right)^{1/2}\right]^{-2} \quad (24)$$

Experiments of Krishna et al. [11] and Ruthiya et al. [12] have shown that increasing catalyst particles concentration decreases gas holdup. The magnitude of holdup decrease cannot be attributed to increase in slurry viscosity or density but rather to increase of large bubble share in bubble population. Since turbulence plays a leading role in coalescence and breakup of bubbles, it seems reasonable to assume that catalyst particles affect turbulence field in liquid component of the slurry and bubble size distribution. Squires and Eaton [13] investigated effect of small particles on isotropic turbulence using DNS. They found that dilute suspension of particles with Stokes number (ratio of particles Stokes time scale to large scale eddy size) ranging from 0.14 to 1.5 tend to attenuate dissipation rate due to preferential concentration of lighter particles (St=0.14-1.5) in areas of low vorticity and high strain rate. Light particles increase small scale

random fluctuations which is equivalent to increased viscous dissipation. Bubble size is affected only by turbulent eddies not exceeding their size – for typical industrial size FT bubble column the Stokes number of catalyst particles calculated as ratio of catalyst particle Stokes time scale and time scale of eddies of bubble size is about 0.25, i.e., particles attenuate dissipation rate of bubble affecting part of turbulence spectrum. As a first order approximation, the effect of catalyst on dissipation rate is accounted for as scaled dissipation rate used as parameter in calculation of average turbulent eddy energy in equation 17. From DNS data for dilute particle suspensions [13]:

$$\bar{e} = 2\left(\varepsilon_{m,scaled}d'\right)^{2/3} = 2\left(\varepsilon_m \cdot e^{-1.2846\alpha_{cat}}d'\right)^{2/3} \quad (25)$$

Equation 28 is valid for dilute catalyst suspensions and Stokes number in range 0.14-1.5. From comparison with experimental data of Krishna et al. (1997) for high catalyst volume fraction it was found that the exponent factor in equation 28 must be modified.

## CFD MODEL

The model described above was implemented into commercial CFD code with Euler multiphase solver [1]. Bubble column operating in churn turbulent regime is characterized by bubble plume oscillation which warrants 3D time dependent approach, [1]. In some cases shallow bubble columns (initial liquid height less than 3-4 column diameters) or bubble columns with intensive gas absorption rate does not exhibit bubble plume oscillation and can be modeled as 2D, axisymmetrical. Renormalization Group Theory [14] version of $k - \varepsilon$ model is strongly advised for 3D calculations because it predicts adequate viscosity which does not dampen natural fluctuation of bubble plume. For 2D calculations a standard $k - \varepsilon$ model [15] is recommended. Inlet boundary at the bottom consists of specification of inlet gas velocity and volume fraction. Outlet boundary condition at the top of bubble column is a constant pressure and backflow value of gas volume fraction must be 1. If gas phase is a mixture of chemical species, a known backflow values of gas species constitute top boundary condition for equation 3. In all examples below the drag coefficient was calculated based on Sauter bubble diameter calculated from known the bubbles size distribution.

## RESULTS AND DISCUSSION

Kulkarni et al. [16] experimented with air water bubble column operating at normal conditions. The inlet gas velocity was 2 cm/sec so the column was operating in bubble flow regime. The inlet bubble diameter was known – 8.8 mm. The bubble size spectrum was split into 10 size classes [1] covering bubble diameter range 1mm-3.8cm. The simulation was run for about 50 seconds with time step size 0.025 sec. Figure 2 displays computational domain and mesh. Figure 3 displays instant and time averaged volume fraction of bubbles. Instant contour shows rolling vortices of liquid creating periodic swarms of bubbles rising up. The time averaged contour is symmetric as expected. The instant water velocity field on Figure 4a confirms existence of rolling vertexes. The time averaged liquid vector field on Figure 4b displays axisymmetric field found in experiment – upward liquid movement in the middle and downward movement

near the wall. Time averaged Sauter diameter on Figure 5 confirms experimentally observed dominance of large bubbles (1 cm diameter) near the center and small bubbles (6 mm) near the wall. This is further confirmed by good agreement with measured Sauter diameter and displayed on Figure 6.
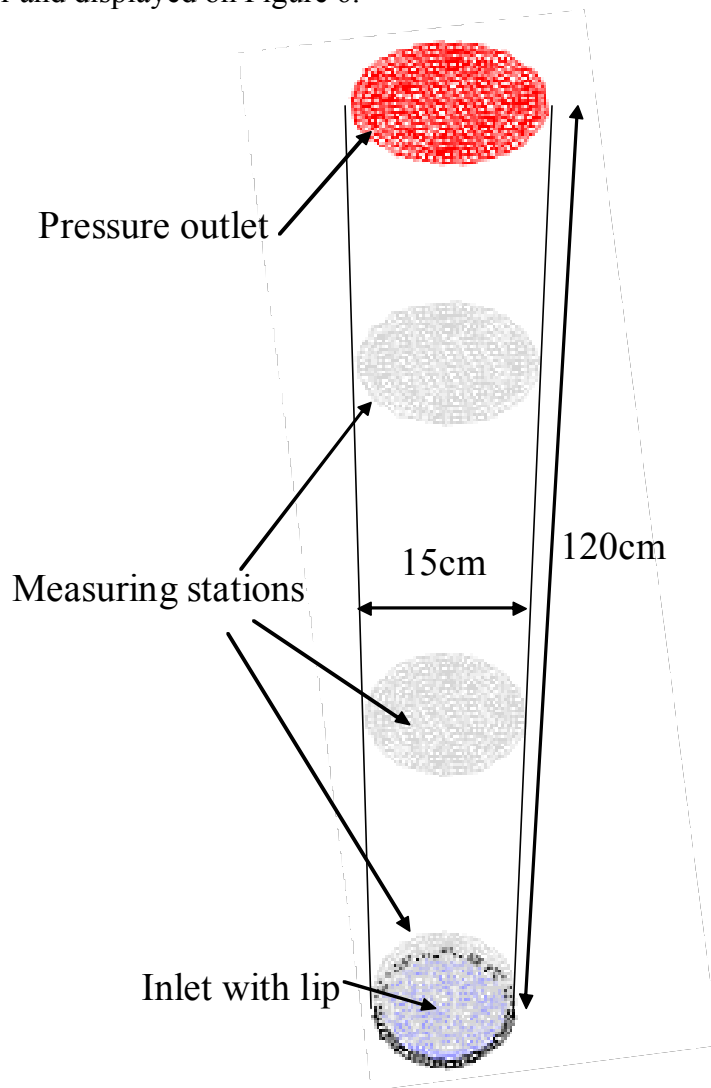


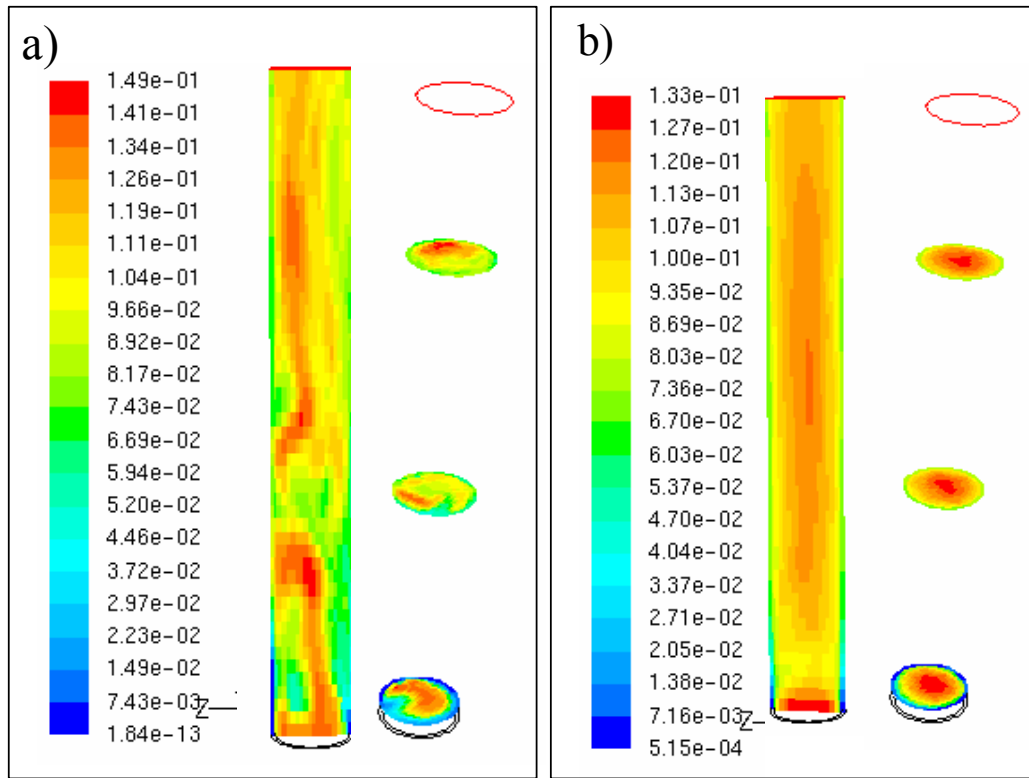Figure 2: Computational domain used in simulation of Kulkarni et al. (2004) experiment.

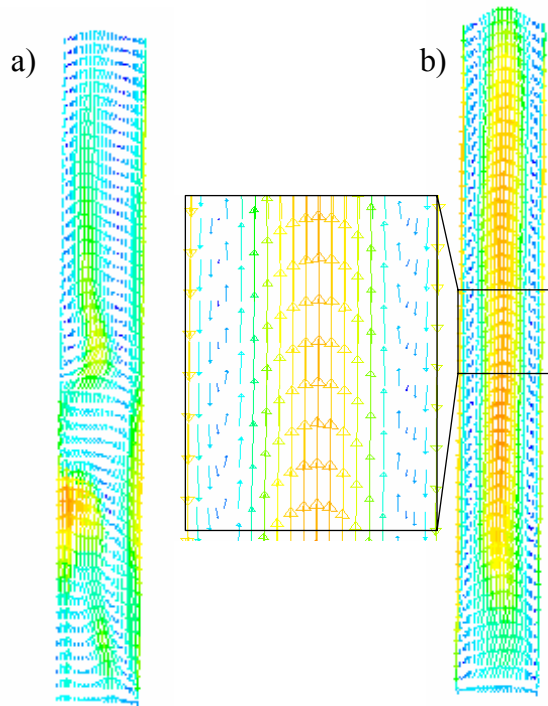Figure 3: Instant (3a) and time averaged (3b) volume fraction of gas bubbles predicted by the model, Kulkarni et al. (2004) experiment.



Figure 4: Instant (4a) and time averaged (4b) water velocity vectors predicted by the model, Kulkarni et al. (2004) experiment.
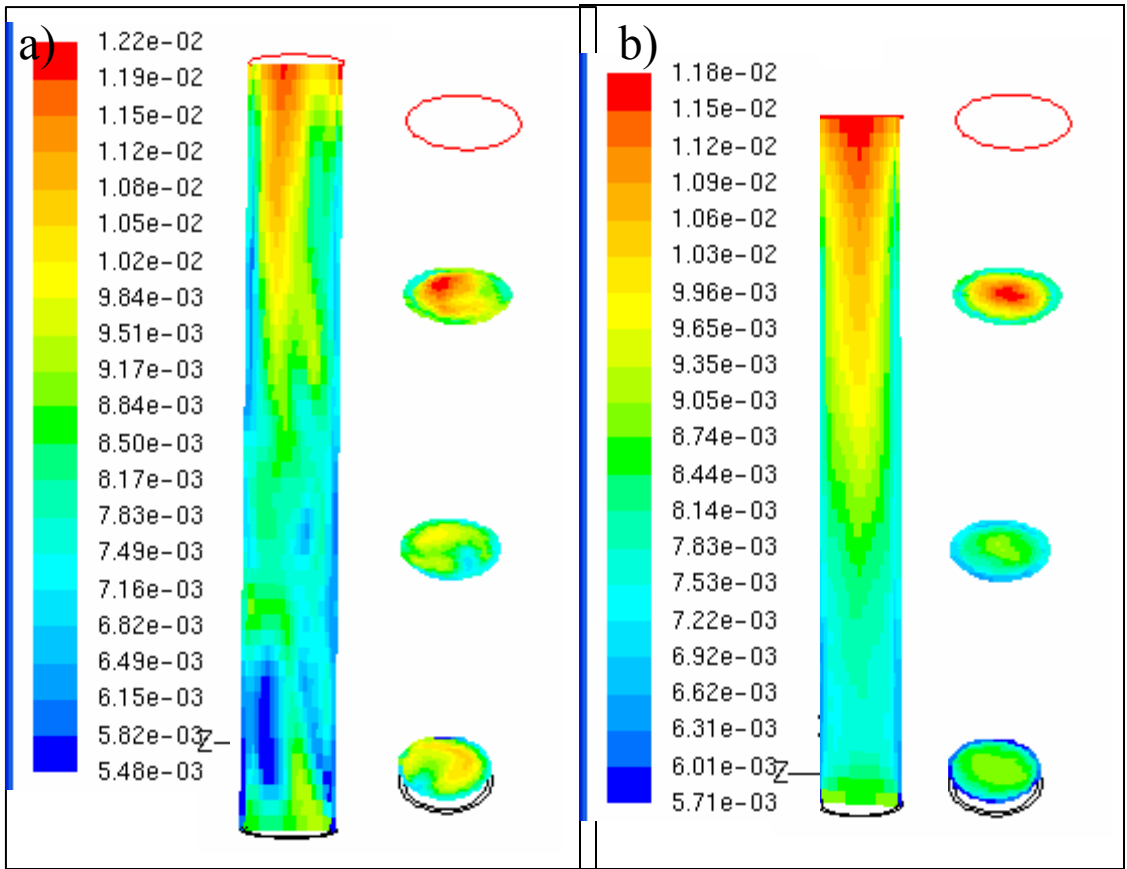
Figure 5: Instant (5a) and time averaged (5b) bubble Sauter diameter predicted by the model, Kulkarni et al. (2004) experiment.
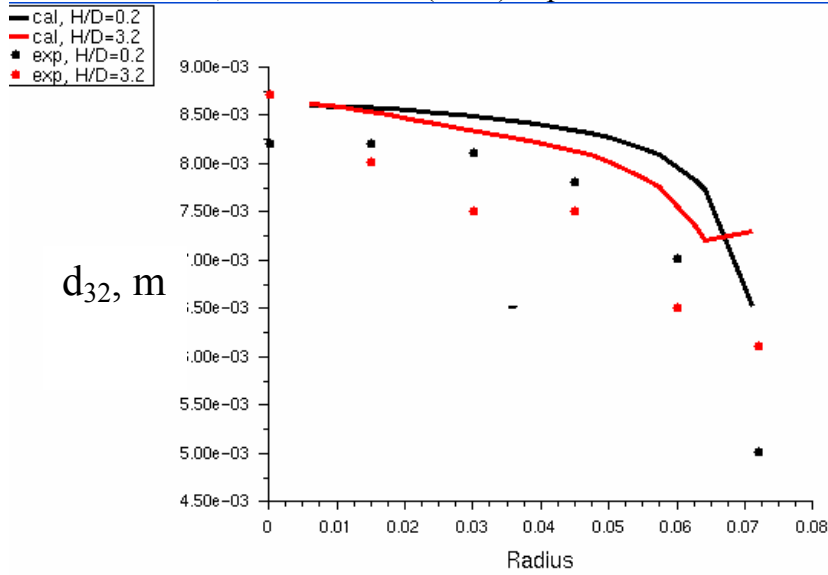


Figure 6: Comparison of predicted and measured time averaged bubble Sauter diameter at different elevations from inlet.

Ability of the model to account for a catalyst concentration effect on the gas holdup (equation 28) was assessed by comparison to experimental data in [11]. The experiment was conducted with ID=0.38 m bubble column. Air bubble and paraffin oil slurry with varying concentrations of 50μ neutrally buoyant particles constituted phases. The computational domain is shown in Figure 7. Comparison of gas holdup vs gas velocity for 0% and 36% catalyst volume fraction is shown in Figure 8. The model correctly predicted the magnitude of catalyst induced holdup reduction at high gas velocity.

Finally, a full 2D time dependent model of FT commercial reactor considered by was run and compared to a 1D lumped parameter model [3]. This is ID=7 m, 30 m height reactor operating at 30 bar pressure and 513K ambient temperature. Chemical species transport and reaction rates described by equations 3-8 were incorporated. Simulations have shown that after initial transient of about 200 sec, a chemical equilibrium established. Simulations were run for gas inlet velocities in range 0.1-0.4 m/s for catalyst volume fraction $\alpha_{cat} = 20\%$ and $\alpha_{cat} = 35\%$. Figure 9 displays two geometries that were investigate. First geometry (Figure 9a) is a simple cylinder where conditions are the same as in 1D calculation for direct comparison to 1D model [3]. Second geometry (Figure 9b) imitates internal structures present in real FT reactor as a cylindrical obstruction in the center.

Figure 10 shows a steady state gas volume fraction for 35% catalyst. At gas velocity 0.1 and 0.2 m/s, the whole gas is absorbed into the slurry so the gas holdup does not change for these flow rates. At gas velocities 0.3 and 0.4 m/s, a portion of gas makes it through the liquid column and presence of axial obstruction increases gas holdup significantly. The holdup increase is caused by formation of wake above the obstruction which enhances liquid mixing and reduced bubble rise velocity due to the drag
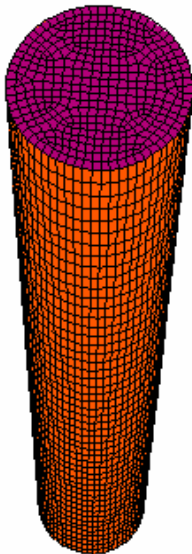


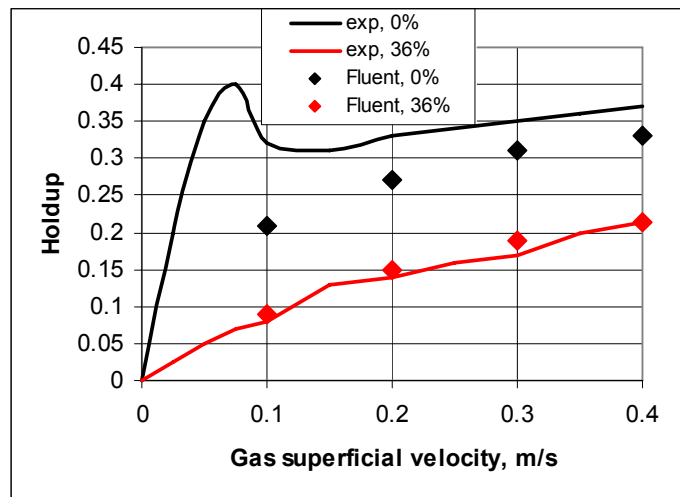Figure 7: Computational grid used for comparison with Krishna at el. (1997).

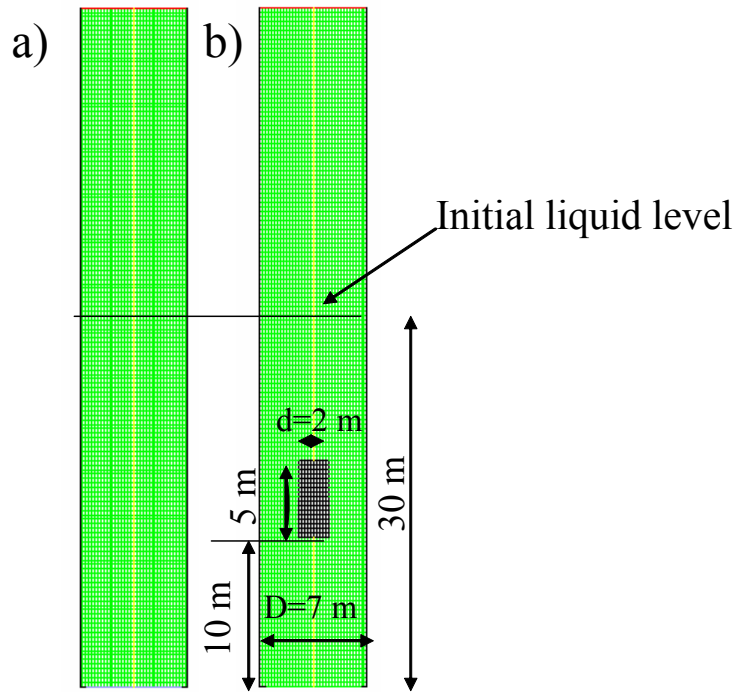Figure 8: Comparison of gas holdup at different catalyst concentration with data of Krishna at el. (1997).

Figure 9: Computational grid used to simulate 2D FT reactor, Maretto and Krishna(1999): a) – without block, b) – with block.
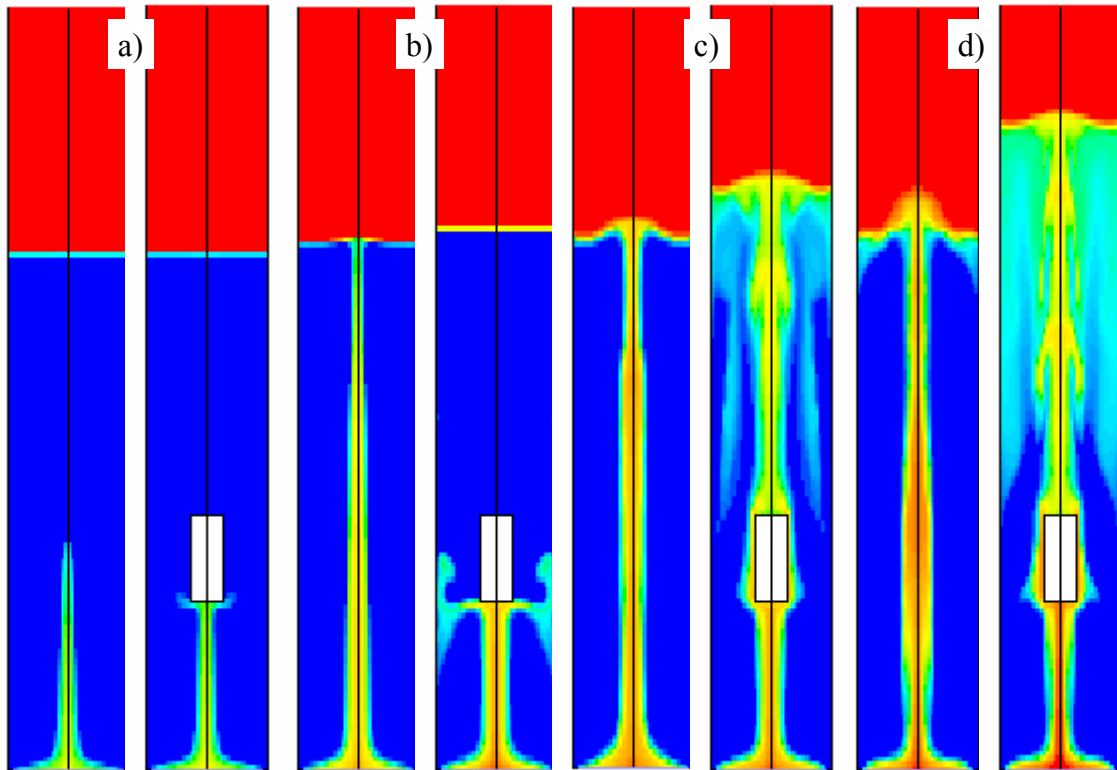


Figure 10: Predicted VOF of gas for 35% catalyst concentration and different gas superficial velocities: a) 0.1 m/s, b) 0.2 m/s, c) 0.3 m/s, d) 0.4 m/s.
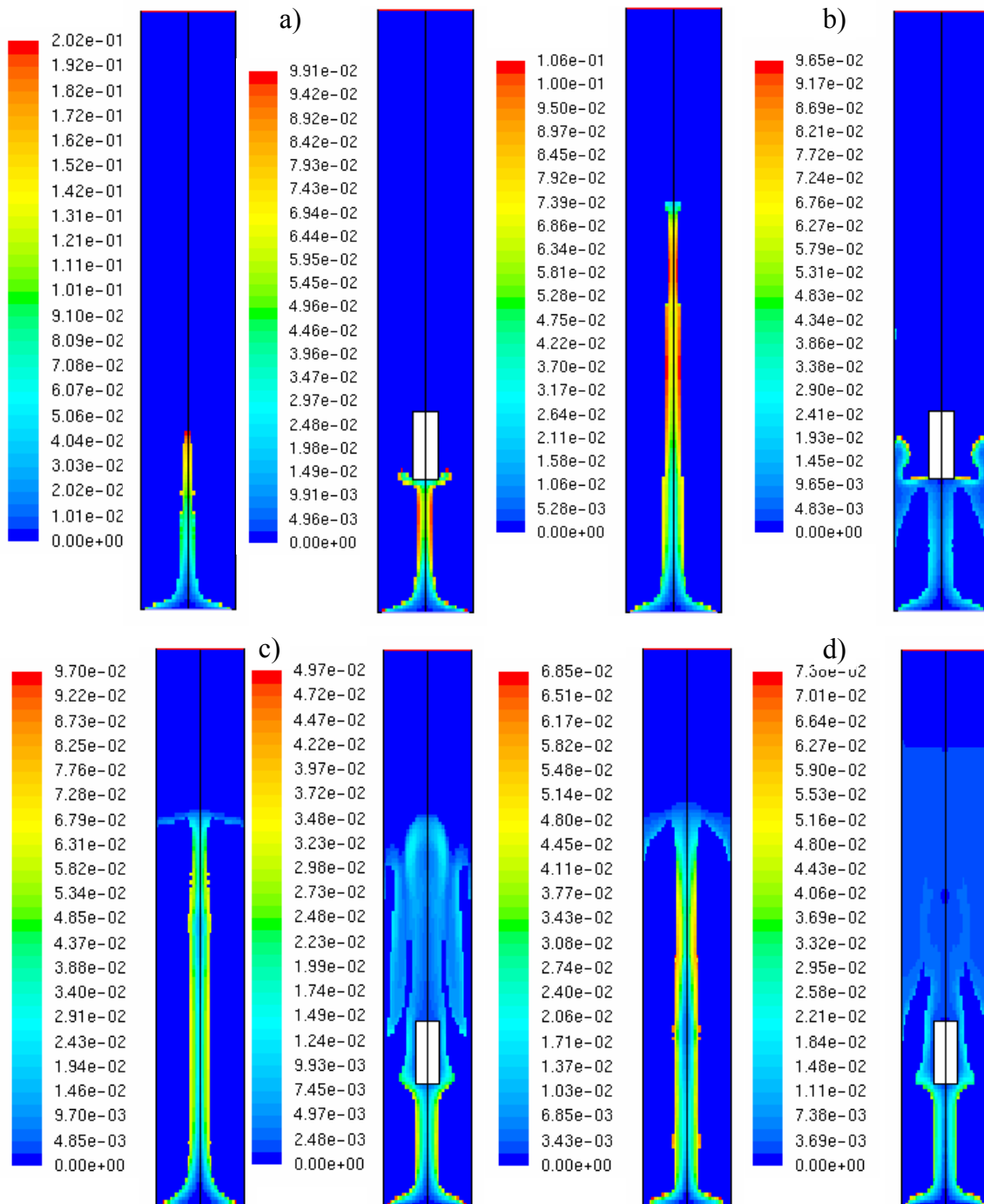
Figure 11: Predicted $H_{2g} \rightarrow H_{2s}$ reaction rate (kmol/m$^3$/sec) for 35% catalyst concentration and different gas superficial velocities: a) 0.1 m/s, b) 0.2 m/s, c) 0.3 m/s, d) 0.4 m/s.

from downward liquid flow. Figure 11 shows reaction rate of hydrogen absorption expressed in equation 5. The absorption happens mostly at the border of bubble plume. Again, the obstruction enhances mixing and makes gas absorption more uniform above the obstruction. Figure 12 shows FT synthesis reaction rate (equation 7). The unblocked reactor configuration shows that maximum FT reaction happens in the center along the
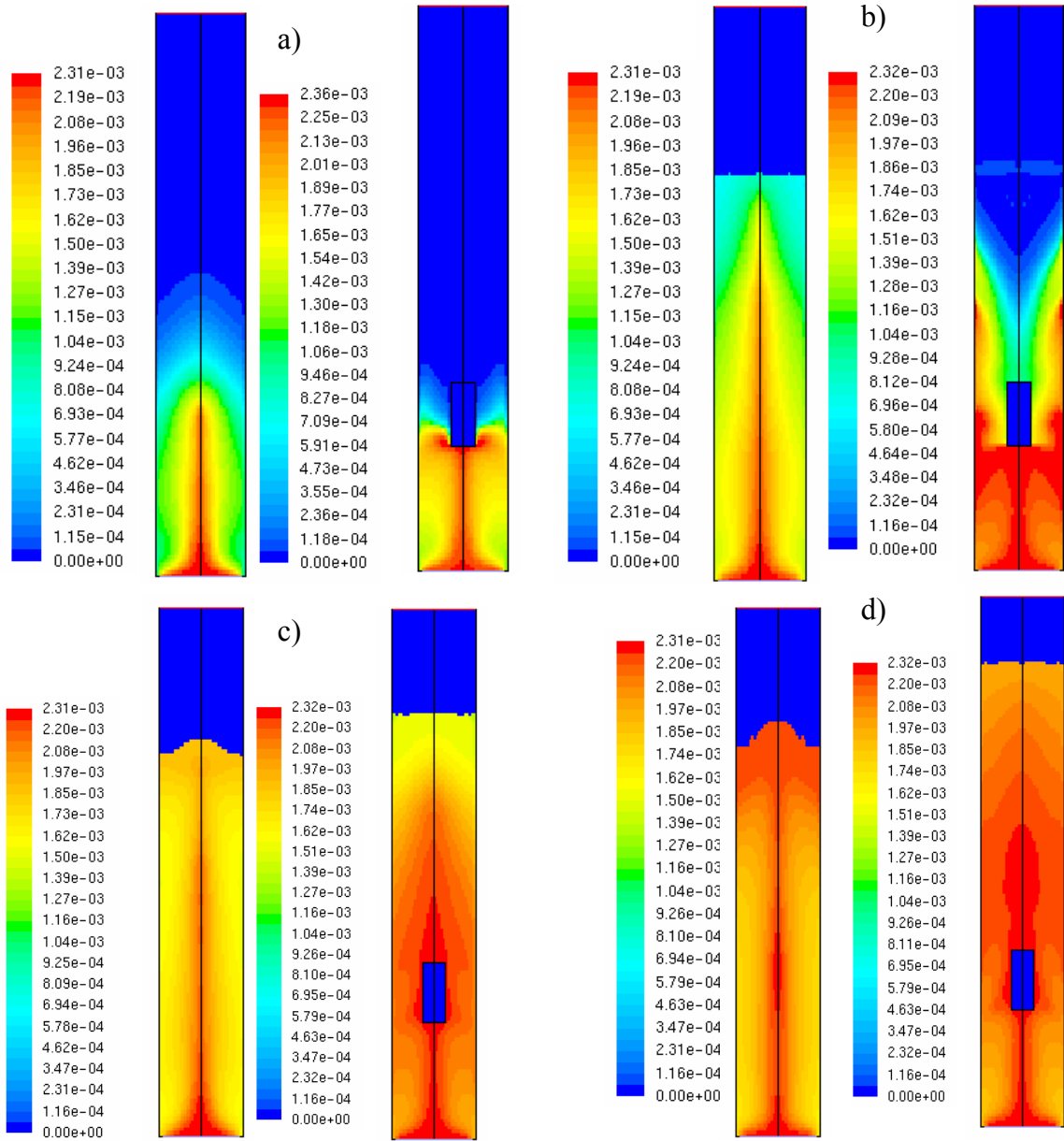
Figure 12: Predicted $2H_{2s}+CO_s\rightarrow CH_{2s}+H_2O_s$ reaction rate (kmol/m$^3$/sec) for 35% catalyst concentration and different gas superficial velocities: a) 0.1 m/s, b) 0.2 m/s, c) 0.3 m/s, d) 0.4 m/s.

bubble plume, i.e., location of gas absorption and ethylene production coincide for unblocked geometry. Presence of blockage introduces recirculation zone in liquid phase and phase separation above the obstruction. This results in distinct maximum in ethylene production at higher gas velocities. Figure 13 displays predicted Sauter diameter. Unobstructed geometry shows expected pattern with larger bubbles near the axis and small bubbles near the wall. The obstruction leads to more inform bubble size distribution above the obstruction.

Figures 14 and 15 display comparison with 1D model of Maretto and Krishna [3] for syngas conversion and ethylene group production, respectively. The CFD
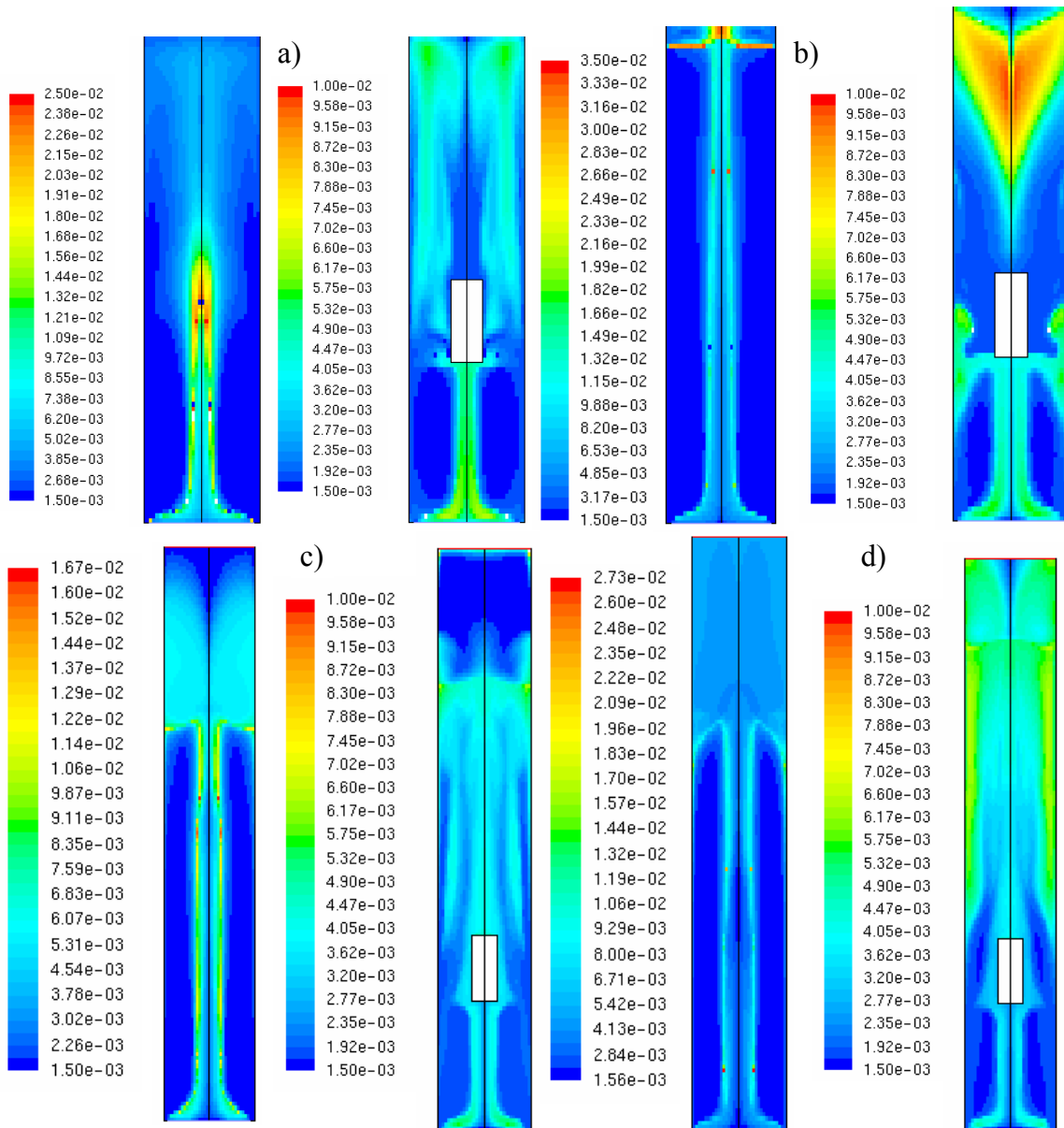
Figure 13: Predicted Sauter diameter for 35% catalyst concentration and different gas superficial velocities: a) 0.1 m/s, b) 0.2 m/s, c) 0.3 m/s, d) 0.4 m/s.

model based on a block free geometry showed reasonable agreement with 1D model. This is expected since the flow is uniform. The agreement is especially good for 35% catalyst concentration. The CFD model predicted higher production of ethylene than 1D model for 20% catalyst concentration. Both CFD and 1D model predicted the same trend in this case – further increase in gas flow rate does not lead to significant increase in production rate unlike in 35% case. This is due to the fact that the process is limited by ethylene production reaction which is not fast enough at 20% to absorb larger bubbles at higher gas velocity.

The blocked geometry introduced increase bubble column production and syngas conversion caused by recirculation above the obstruction.
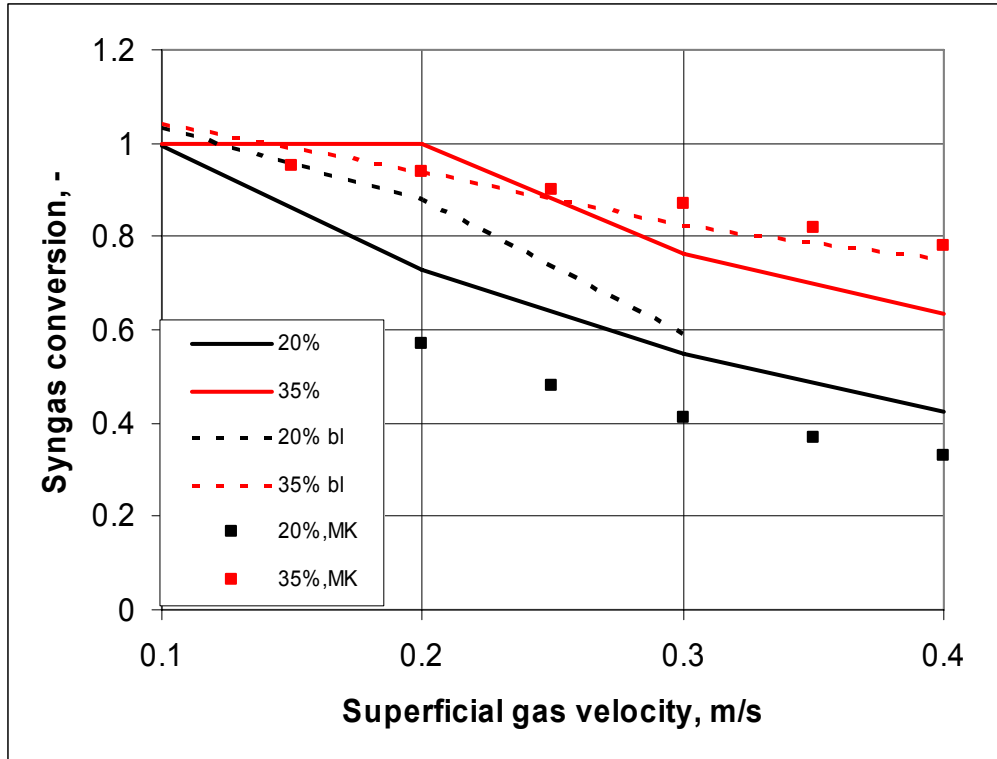
Figure 14: Comparison of CFD predictions of syngas conversion with 1D model predictions of Maretto and Krishna (1999).
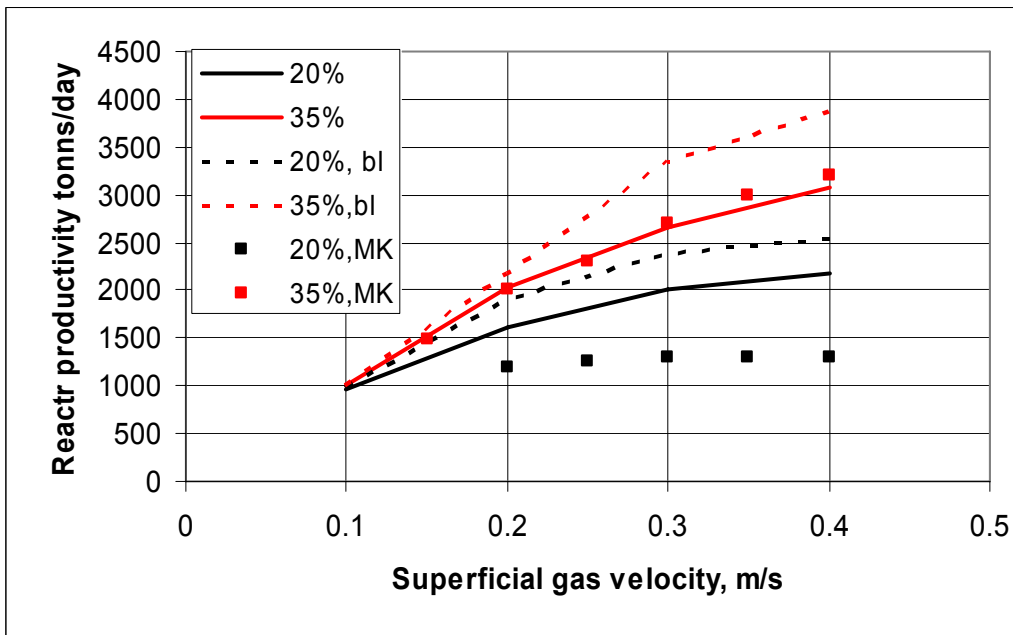


Figure 15: Comparison of CFD predictions of FT reactor ethylene productivity with 1D model predictions of Maretto and Krishna (1999).

## CONCLUSIONS

A realistic CFD model of Fischer-Tropsch reactor was built and validated against experimental data and other 1D calculation. The model includes advanced Population Balance method to compute bubble size distribution and drag law. A simple model for catalyst concentration influence of bubble size is introduced and validated against available experimental data. The model is based on the assumption of suppression of turbulent eddies of the size of bubbles by catalyst particles. A mass conservation of chemical species associated with phases and chemical reactions are solved together with homogeneous and heterogeneous reactions. A CFD predicted productivity of the model for the industrial scale cylindrical FT reactor compared well with simple 1D semiempirical model. The blocked geometry imitating internal reactor structures which cannot be simulated in 1D was also explored. It was found that recirculation zone introduced by blockage increases mixing and enhances productivity of the reactor.

## NOTATION

| | |
|---|---|
| $A_{gs}''$ | Interfacial area density, 1/m |
| $C_{gs}^d$ | drag coefficient |
| $c$ | molar concentration of species, (kmole/m$^3$/sec) |
| $D_q^j$ | diffusion coefficient of species $j$ in phase , kg/m/s |
| $d_i$ | bubble diameter (m) |
| $f_i$ | fraction of bubbles of class i |
| $\vec{g}$ | gravity vector |
| $H$ | Henry constant |
| $K_{pq}$ | phase exchange coefficient between phases $p$ and $q$ (Ns/m$^4$) |
| $k$ | turbulent kinetic energy (m$^2$/s$^2$) |
| $(k_L a)$ | volumetric mass transfer coefficient, (1/s) |
| $\dot{m}_{gsi}$ | mass transfer rate between bubble classes due to interfacial mass transfer, (kg/m3/sec) |
| $n_i$ | bubble number density of class $i$, 1/m$^3$ |
| $p$ | pressure (Pa) |
| $S_{gi}$ | Mass exchange rate due to coalesce and breakup, (kg/m3/sec) |
| $S_q^j$ | mass exchange rate due to homogeneous reaction, (kg/m3/sec) |
| $S_{qp}^{lj}$ | mass exchange rate due to heterogeneous reaction, (kg/m3/sec) |
| $\vec{v}_q$ | velocity vector of phase $q$, m/s |
| $Y_q^j$ | mass fraction of species $j$ in phase $q$ |
| $\alpha_k$ | volume fraction of phase $q$ |
| $\varepsilon$ | turbulent dissipation rate (m$^2$/s$^3$) |
| $\rho_k$ | density of phase $k$ (kg/m$^3$) |

| | |
|---|---|
| $\sigma_{sg}$ | surface tension (N/m) |
| *Sub* | |
| *cat* | catalyst phase |
| *g* | gas phase |
| *m* | mixture |
| *s* | slurry phase |

## REFERENCES

1.      Chen, P. et. al, (2005) "Numerical simulation of bubble columns flows: effect of different breakup and coalescence closures", *Chemical Engineering Science* Vol. 60, pp. 1085-1101.

2.      Saxena S. (1995) "Bubble column reactors and Fischer-Tropsch synthesis", *Catal. Rev.-Sci. Eng.* Vol. 37, (2) pp. 227-309.

3.      Maretto, C. and Krishna, R. (1999) "Modelling of a bubble column slurry reactor for Fischer-Tropsch sythesis" *Catalysis Today* Vol. 52, pp. 279-289.

4.      Yates, I. and Satterfield C. (1991) "Intrinsic kinetics of the Fischer-Tropsch synthesis on a cobalt catalyst" *Energy & Fuels* Vol. 5, pp. 168-173.

5.      Ishii M. and Mishima K. (1984) "Two-fluid model and hydrodynamic consituitive relations", *Nuclear Eng. And Design* Vol. 82, pp. 107-126.

6.      Luo, H., "Coalescence, breakup and liquid circulation in bubble column reactors", Ph.D. Thesis, Universitetet I Trondheim, Norges Tekniske Hgskole, 1993.

7.      Lehr F. et al. (2002) "Bubble-size distributions and flow fields in bubbles columns", *Fluid Mechanics and Transport Phenomena* Vol. 48, (11) pp. 2426-2443.

8.      Hinze J. (1955) "Fundamentals of the hydrodynamic mechanism of splitting in dispersion processes", *AIChE Journal* Vol. 1, (2), pp. 289-295.

9.      Kolev N. (2005) "Multiphase flow dynamics: vol 2", *Springer-Verlag* p. 247.

10.     Ishii M. and Zuber N. (1979) "Drag coefficient and relative velocity in bubbly, droplet and Particulate flows", *AIChE Journal* Vol. 25, (5).

11.     Krishna R. at el.  (1997) "Gas holdup in slurry bubble columns: effect of column diameter and slurry concentrations" *AIChE J.* Vol. 43, 2 pp. 311-316.

Krishna R. et al. (1998) "Scale effects in fluidized multiphase reactors" *Chem Eng Sci* Vol. 54 , pp. 4903-4911.

12.     Ruthiya K. et al. (2006) "Influence of particles and electrolyte on gas holdup and mass transfer in slurry bubble column", *Int J. of Chemical Reactor Eng.* Vol. 4, (A13) pp. 1-35.

13.     Squires, K. and Eaton, J, (1994) "Effect of selective modification of turbulence on two-equation models of particle-laden flows", *J. of Fluids Engineering* Vol. 116, pp. 778-784.

14.     Yakhot, V. and Orszag S. A. (1986) "Renormalization group analysis of turbulence I: Basic Theory" *Journal of Scientific Computing* Vol. 5, 1 pp. 1-51.

15.     Launder B. E. and Spalding D. B. (1974) "The numerical compution of turbulent flows", *Comp. Meth, Appl. Mech.* Vol. 3, (11) pp. 269-289.

16.     Kulkarni A. et al. (2004) "Determination of bubble size distributions in bubble columns using LDA", *AIChE Journal* Vol. 50, (12) pp. 3068-3084.